Batteries & Supercaps

Research Article
doi.org/10.1002/batt.202500421

Chemistry Europe
European Chemical Societies Publishing

www.batteries-supercaps.org

Understanding the Temperature–Induced Decomposition of Commercial Nickel–Cobalt–Aluminum Oxide ($LiNi_{0.8}Co_{0.15}Al_{0.05}O_2$) Electrodes

Tobias Hölderle, Volodymyr Baran, Alexander Schökel, Lea Westphal, Robert U. Stelzer, Rainer Niewa, Peter Müller-Buschbaum, and Anatoliy Senyshyn*

This study addresses the thermal degradation and structural stability of the NCA (nickel–cobalt–aluminum oxide) cathode materials under varying states of charge (SOC)/delithiation and temperature. Using simultaneous thermogravimetric and differential thermal analysis and high-resolution X-ray diffraction, the sequential evolution from a layered $NaCrS_2$-type structure to spinel phases (M_3O_4-type and LiM_2O_4-type) and finally to a rock salt phase is characterized. Degradation involves cation migration, oxygen release, and lattice instabilities, influenced by SOC/lithium content. Fully lithiated NCA (SOC 0%) exhibits superior thermal stability with a single-step transition, whereas partially delithiated NCA exhibits a multistep transformation process involving spinel intermediates. These findings highlight the complex interplay between energy density and thermal safety, offering guidance for designing NCA cathodes with optimized performance, safety, and stability for high-energy lithium-ion batteries.

1. Introduction

Lithium-ion batteries (LIBs) have become irreplaceable in modern energy storage applications, ranging from portable electronics to electric vehicles, due to their high energy density, long cycle life, and versatility.[1] The performance and longevity of LIBs are influenced not only by the type of electrolyte[2,3] and anode material[4–6] but also significantly by the type of cathode material.[7] Over the years, cathode materials have evolved in chemical composition and morphology to meet the increasing demands for higher energy densities, improved thermal stability, and extended cycle life, such as lithium cobalt oxide ($LiCoO_2$, LCO), introduced in the 1980s and used in the first patented LIB as cathode material.[8,9] However, LCO suffered from pronounced safety issues (due to the reactive character of the CoO_2 compound) and limitations in high costs, resulting in the introduction of the $LiNiO_2$ cathode, substituting the cobalt with nickel.[10] While this material is beneficial in terms of safety, it shows accelerated capacity fading, poor thermal stability and decreasing rate capability, leading to the development of various advanced layered oxides $LiMO_2$ (M = Ni, Co, Mn, Al) with tunable composition, such as nickel–manganese–cobalt oxide (NMC) cathodes, and/or nickel–cobalt–aluminum oxide (NCA) cathodes (e.g., $LiNi_{0.8}Co_{0.15}Al_{0.05}O_2$).[11] NCA has gained in popularity due to its high nickel content, which enhances specific capacity and energy density, while the addition of cobalt and aluminum stabilizes the crystal structure.[12] However, the high nickel content also faces critical safety and structural degradation challenges, making the NCA material vulnerable to thermal degradation, especially at an elevated state of charge (SOC), where delithiation disrupts the cathode structure.[13,14] In particular, the thermal stability of the cathode material plays a key role in ensuring battery safety, becoming especially important during fast charging, which can introduce significant local heat to NCA cathodes, due to Joule heating caused by increased local current densities. Besides the heating up at the LIB level, it also creates thermal gradients across the electrodes, leading to nonuniform degradation.[15] In addition, the heat generation can trigger exothermic chemical reactions in the electrodes, similar to those reported in ref. [16] for delithiated graphite anodes. Similar reactions can occur at the positive electrode, leading to oxygen and other volatile gases release,[17,18] due to the reduction of Ni^{4+} to Ni^{2+} in NCA cathodes, further increasing the risk of battery failure leading to thermal runaway.[19–21] In general, the deterioration of charged

T. Hölderle, L. Westphal, P. Müller-Buschbaum, A. Senyshyn
Department of Physics
Chair for Functional Materials
TUM School of Natural Science
Technical University of Munich
James-Franck Str. 1, 85748 Garching, Germany
E-mail: anatoliy.senyshyn@frm2.tum.de

T. Hölderle, V. Baran, L. Westphal, A. Senyshyn
Heinz Maier-Leibnitz Zentrum (MLZ)
Technische Universität München
Lichtenbergstr. 1, 85748 Garching, Germany

V. Baran, A. Schökel
Deutsches Elektronen Synchrotron DESY
Notkestr. 85, 22607 Hamburg, Germany

R. U. Stelzer, R. Niewa
Institute of Inorganic Chemistry
University of Stuttgart
Pfaffenwaldring 55, 70569 Stuttgart, Germany

Supporting information for this article is available on the WWW under https://doi.org/10.1002/batt.202500421

NMC and NCA materials follows a particular degradation sequence during heating. At room temperature, the electrode active material has a stable layered structure, showing a phase transition during heating via a spinel phase to a rock salt phase,[22,23] as suggested by temperature-dependent neutron and X-ray diffraction studies focused on the structural degradation of NMC and NCA structures. The effect of composition in NMC structures on the thermal structural stability was investigated in detail in ref. [24], showing that a subtle balance of Ni, Co, and Mn ratios significantly influences thermal degradation of these materials. While a high nickel content (NMC 811) decreases the structural stability, a lower nickel content (NMC 333) plays a positive role in thermal stability, but typically at the cost of reduced capacity.[25] In addition, the amount of lithium in the cathode structure can influence the structural behavior upon heating, resulting in faster degradation of deeply delithiated NCA materials.[26] However, the degradation path for NCA cathodes is only explored for selected delithiated compositions. All this requires and deserves more detailed consideration and characterization of the effects of temperature on NCA cathode materials in the entire range of SOC typical for real applications. The SOC-dependent thermal stability of cathodes is critical because of the complex interplay of different degradation mechanisms playing different roles at varying degrees of delithiation. At low SOCs, the cathode shows higher structural stability at room temperature and possibly a higher resistance to thermal degradation. On the contrary, at high SOCs, the cathode tends to become structurally unstable, with increased risks of oxygen release, lattice collapse, and thermal runaway.[13,27] In addition, operating at low temperatures is associated with a specific set of challenges: at subambient temperatures, the kinetics of lithium-ion diffusion and charge transfer are considerably hindered, resulting in increased resistance and reduced capacity.[28] Thus, the combined effects of low-temperature operation followed by high-temperature exposure, such as during fast charging, can cause thermal stress and lead to cumulative degradation. Therefore, a detailed investigation into low- and high-temperature behavior is essential for developing advanced cathode materials. In the current contribution, the temperature-dependent degradation of real-life NCA cathodes across the full SOC range is investigated in detail. The electrodes were harvested from LIBs and systematically studied using a combination of diffraction techniques and gravimetric and calorimetric methods.

2. Results and Discussion

A pronounced degradation of NCA cathodes occurs at high temperatures, showing a cascade of transformations from a layered phase toward a spinel phase and then to a rock salt phase. The transition sequence is similar for all SOCs. In the initial state at ambient temperatures, the layered-type is built up from alternating transition metals/aluminum layers and layers of lithium ions occupying the octahedral sites, and separated by an additional oxygen layer ($[Li/M]O_2$-layers), showing an ABCABC stacking sequence.[13,29] During electrochemical delithiation, transition metals, such as Ni and Co, undergo oxidation, typically transitioning from a mixed 2+/3+ state toward higher oxidation states, with Ni oxidizing through an intermediate Ni^{3+} state to the Ni^{4+} state, and Co oxidizing from Co^{3+} toward Co^{4+}, while the oxidation state of Al^{3+} remains unchanged and stabilizes the structure. However, this does not affect the content of the Ni, Co, and Al in the NCA structure, which stays constant across the whole range of SOCs. On the contrary, when heating the NCA at high charging states, the Ni and Co ions experience a reduction from Ni^{4+} toward Ni^{2+} and Co^{3+} to Co^{2+}, supplemented by a simultaneous oxygen release.[18,24,30] Excessive cation migration can result in the disordered LiM_2O_4-type, where mostly Ni ions migrate from their initial site toward the octahedral site in the Li-slabs through the energetically more favorable nearest tetrahedral site. At the same time, Li-ions are moving from their octahedral sites in the layered structure to the tetrahedral sites in the LiM_2O_4 structure.[24,31] Alternatively, cation migration can lead to the M_3O_4-type spinel phase, where the Co ions follow the migration of the Ni ions and partially occupy the 8a tetrahedral sites of the M_3O_4-type structure. Remarkably, the occurrence of 220/422 spinel reflection intensities is a reliable indicator of such an M_3O_4-type phase.[26] Further heating promotes the transition from a spinel to a more stable rock salt phase, leading to the migration of Li and transition metals to the adjacent octahedral site in the rock salt structure. Thermal gravimetric analysis (TGA) probed the degradation sequence in various delithiated NCA cathodes at high temperatures under an inert argon atmosphere (**Figure 1**a). With rising temperatures, the cathode material experiences a significant weight loss, occurring in two steps. While the first step is relatively small and similar for all SOCs ($<\Delta m/m> = 2.5\%$), the second weight loss step shows remarkably higher values, which increase with decreasing amount of lithium in the NCA structure (Figure 1a). Observed behavior is associated with the release of oxygen from the structure caused by a series of phase transitions from a layered NCA material (α-$NaCrS_2$-type) over the spinel (ordered LiM_2O_4-type or disordered M_3O_4-type) to a NaCl-type structure.[18,32] The delithiation degree of the NCA material defines the amount of oxygen released and the temperature at which the phase transition occurs. However, for samples greater than 20% SOC, a two-step series is present, where each step represents the release of oxygen, representing the phase evolution of NCA. Contrary, the fully discharged NCA structure shows only a single step, marking a continuous phase transition from a layered over a spinel to a rock salt phase. The weight loss of the NCA structure can be described as linearly increasing with decreasing lithium in the structure (Figure 1b). To quantify oxygen-related weight loss, we calculated the mass of oxygen released during each step relative to the theoretical molar mass of the NCA composition at each SOC (Table S1, Supporting Information). The molar mass was determined by the incorporation of variable lithium concentrations at each SOC, based on refined lithium occupations obtained from full-profile Rietveld analysis at 300 K (Table S2, Supporting Information). The initial oxygen content is defined as two moles of oxygen per formula unit, and deviations from this are interpreted as evolved oxygen. Thus, at 0% SOC, the calculated oxygen loss is $\approx 6.25\ g\ mol^{-1}$. As lithium content decreases with charging, the oxygen loss increases, reaching a maximum of

Research Article
doi.org/10.1002/batt.202500421
Chemistry Europe
European Chemical Societies Publishing

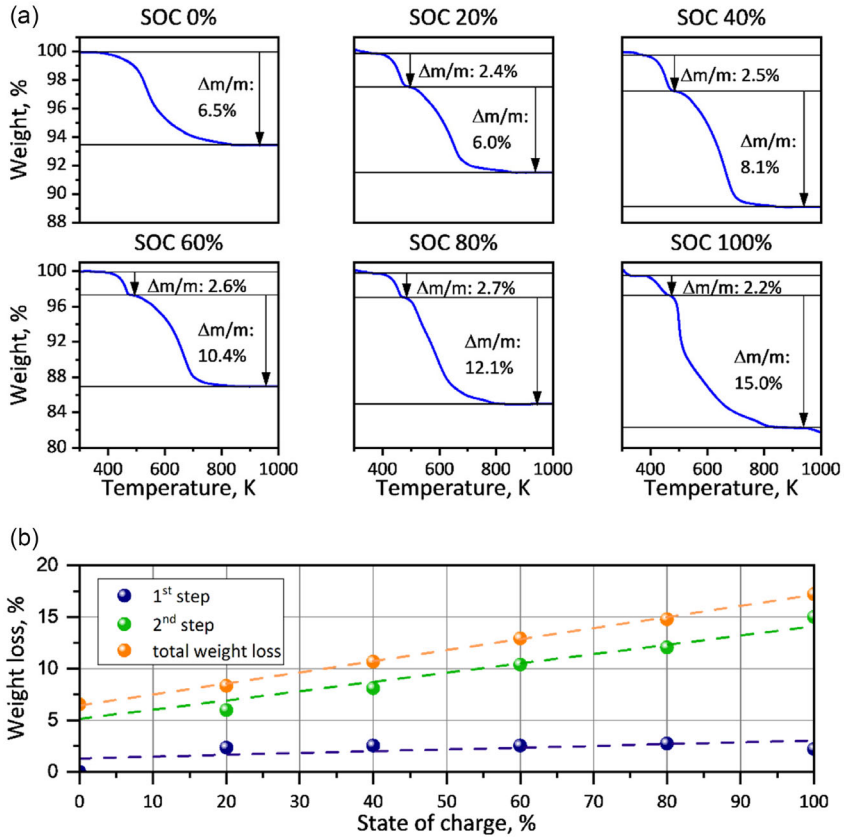

Figure 1. a) Weight loss of the NCA cathodes upon heating for different delithiated NCA compositions ranging from SOC 0% to SOC 100%. b) The weight loss of different structures is carried out by a two-step process, dependent on the SOC, with parameters written in Table S1.

≈15.68 g mol^{-1}. A small portion of the measured mass loss may result from lithium undergoing side reactions with the sample container. However, the dominant contribution to the mass loss is attributed to the lattice oxygen release, consistent with the previous reported thermal behavior of Ni-rich layered oxides.[18,24,26] Note, the loss of oxygen is a well-known issue within lithium transition metal oxide derivatives, which is not only dedicated to thermal effects but also driven by the delithiation and side reactions with the electrolyte, resulting in the observed phase transformations, mechanical cracking, and oxygen vacancies. Thus, higher delithiation of the NCA results in an increasing oxygen release and oxygen vacancies, destabilizing the NCA structure.[33]

Besides TGA, differential thermal analysis (DTA) measurements revealed an exothermic behavior of the phase transitions for all SOCs upon heating (Figure S1, Supporting Information). While the NCA in a fully delithiated state displays a single exothermic peak at 870 K along with the single weight loss step and the formation of the rock salt phase, higher delithiated NCA structures show multiple thermal signals at different positions. The first two peaks appear in the temperature range 450–550 K, getting more pronounced with increased delithiation and indicative of a transition from the layered-type to the spinel-type structure. The third pronounced peak appears at 850–950 K, attributed to a transition to the rock salt-type structure, which is stable and shows no further transitions upon cooling. Complementary to TGA/DTA measurements carried out in argon atmosphere, measurements in synthetic air were carried out to account, and differentiate between the potential influences of oxidative degradation conditions on the thermal decomposition behavior of NCA measurements. The measurements showed that the overall behavior in synthetic air is qualitatively similar to that observed in argon atmosphere (Figure S2, Supporting Information). While the mass loss steps and exothermic peaks observed in synthetic air measurements show minor differences to the ones measured in argon, the sequence of degradation remains the same. Thus, such small differences suggest that there is little to no residual carbon present, which would react in the presence of air and show significant mass loss steps in the TGA data during heating. Alternatively, such carbon could be oxidized at temperatures above 1000 K. However, such experiment confirmed that the observed thermal effects below 1000 K originate from the lattice oxygen release and phase transitions rather than from side reactions of carbon impurities.

In addition to the thermal analytics, high-resolution X-ray powder diffraction measurements were carried out at high and low temperatures on NCA samples sealed airtight within an argon-containing glovebox to probe the observed phase transitions in detail. In **Figure 2**, the thermal behavior of selected NCA compositions at high temperatures is shown, directly linked to its phase transitions and structural stability imparted by its ingredients (remaining data in Figure S3, Supporting Information).

Research Article
doi.org/10.1002/batt.202500421
Chemistry Europe
European Chemical Societies Publishing

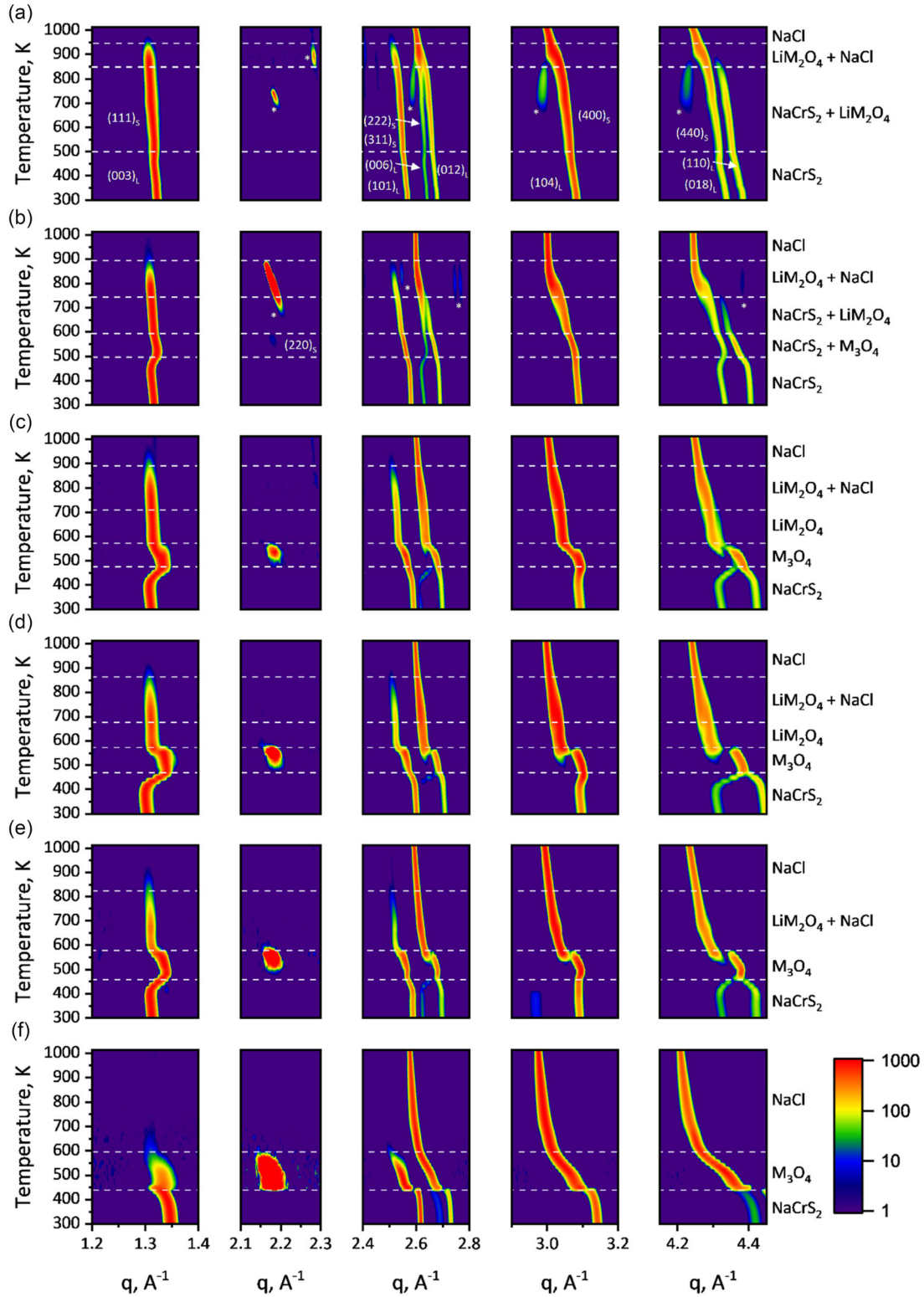

Figure 2. Structural evolution of characteristic reflections for differently delithiated NCA at SOC a) 0% b) 20% c) 40% d) 60% e) 80%, and f) 100%, showing thermal degradation. Bragg indices are indicated in a) at different positions, dashed lines highlight the corresponding phase transition, while superstructure reflections are marked with asterisks.

In general, a pattern of degradation consistent with thermoanalytic measurements was observed. At ambient temperatures, the NCA material displays a layered rhombohedral $NaCrS_2$-type structure, as shown by the appearance of characteristic Bragg reflections (marked by a subscript L), such as $(003)_L$, $(108)_L$, and $(110)_L$, which are present for all SOC but occur at different positions caused by varying SOC (Figure S4, Supporting Information). The change of the peak position reflects the

extraction of lithium ions from the NCA structure during the electrochemical cycle, resulting in the change of lattice parameters. The observed structural changes for different delithiation stages (SOC = 0–100%) were analyzed, and the lattice parameters (Table S2, Supporting Information) were extracted using the full-profile Rietveld refinement method with the program suite FullProf[34] (Figure S5, Supporting Information). I.e., upon delithiation of the initial NCA structure (SOC = 0%), the c lattice parameter shows an almost linear expansion with increasing SOC, reaching its maximum around 70% SOC (Figure S6, Supporting Information). Afterward, a strong contraction of the c parameter occurs, decreasing below its initial value and indicating significant structural changes at high degrees of lithium extraction. This behavior is already well-known and described by ref. [13]. Thus, the c parameter behavior is often considered as a destabilizing factor in the NCA structure, decreasing thermal stability with increasing delithiation, due to the increasing number of voids and increased oxidation states of the transition metals.[35,36]

Increasing temperatures result in the emergence of a spinel phase for all delithiated NCA compositions, which is reflected by the shift of $(018)_L$ and $(110)_L$ reflection couple toward each other (Figure 2). The formation of the spinel phases follows different routes, where transition temperatures are decreased with lowering lithium concentration. At SOC = 0%, the LiM_2O_4-type spinel phase evolves first, whilst at higher SOCs a transition to the intermediate M_3O_4-type spinel phase occurs (supplemented by the appearance of dedicated $(220)_S$ reflection at low q and the $(422)_S$ reflection at higher q, Figure S7, Supporting Information). In addition, the $(111)_S$ reflection is actively shifting toward higher q values. This can be attributed to the higher structural stability at low SOC, suppressing the formation of the M_3O_4-type spinel and resulting in the occupation of the tetrahedral positions of the spinel phase only by the Li-ions, with transition metals located at the octahedral sites. In contrast, the emergence of the M_3O_4-type spinel resulted from increased cation mobility in the NCA structure, enabled by the lithium deficiency. With a lower amount of Li in the NCA material, voids are introduced into the structure, which, in line with the increase in oxidation states of the Ni and Co ions, destabilize the layered NCA structure.[13] In turn, it further increases cation mobility, resulting in the partial migration of Co ions toward the tetrahedral sites of the spinel framework, visible by the appearance of characteristic $(220)_S$ reflection. Observed structural transition is known to be accompanied by a substantial oxygen gas evolution (associated with the loss of oxygen from the lattice to accommodate the redistribution and reduction of the transition metal oxidation states). The release of oxygen supplements the phase evolution, and it is observed as the first weight loss step in the TGA data for SOCs > 20%. However, this step is lacking during the phase transition to the LiM_2O_4-type spinel.[24,26] Thus, at SOC 0%, the missing initial weight loss step indicates the absence of instantaneous oxygen release, showing a more continuous weight loss in a single step during heating and the transition toward a LiM_2O_4-type spinel phase.[23] Furthermore, for increased delithiation states up to SOC 20%, a mixed phase composed of M_3O_4-type spinel and the initial layered-type structure was observed, while the pure M_3O_4-type spinel phase evolves at SOCs ≥ 20%. Further heating of the structure results in the transition from the M_3O_4-type to the thermodynamically more stable LiM_2O_4-type spinel phase, as indicated by the vanishing of the $(220)_S$ reflection, which requires an additional redistribution of the Co ions from the tetrahedral site to the octahedral site. While for SOCs below 20%, the spinel phase coexists with residues of the layered NCA-type, a direct transition to a pure LiM_2O_4-type spinel phase is observed for 20% > SOCs < 70%. At SOCs > 70%, a transition from the M_3O_4-type to a mixed phase of the LiM_2O_4-type spinel and the energetically favored NaCl-type structure is reached directly. The same phase is present after further heating of SOCs ≤ 70% at higher temperatures. Note: while this phase is observable for the majority of SOCs, it does not occur in the dataset for the fully delithiated NCA structure.

The final phase transition represents the spinel-to-NaCl-type phase transformation at higher temperatures, where the vanishing of the $(111)_S$ and $(311)_S$ reflections is indicative. Besides this, it proceeds with the appearance of superstructure reflections, which are especially prominent at low SOCs in the vicinity of the phase transition to the rock salt structure. These reflections indicate the cation rearrangement within the lattice, suggesting an unstable spinel phase, which could result in the intermittent transition to the lower symmetry ordered rock salt structure at higher temperatures. As heating continues, the cations undergo further migration, resulting in a random occupation of the octahedral sites in the rock salt-type structure, accompanied by the collapse of the oxygen framework. This, in turn, results in metastable high oxidation state transition metal oxides, which tend to release oxygen,[26] visible in the second weight loss step of the TGA data for all SOCs. This phase transition occurs at progressively lower temperatures with increasing delithiation state of the NCA structure. While the phase transition to the NaCl-structure type is observed at ≈ 950 K in a fully lithiated state, it is lowered to ≈ 600 K in a fully delithiated state. This dependency highlights the stabilizing role of the lithium ions on the NCA structural framework, as their presence reduces the mobility of cations and the amount of released oxygen.[23] At low SOCs, the layered NCA structure displays a remarkable stability of up to ≈ 850 K, as revealed by the characteristic $(110)_L$ reflection.

It is essential to mention that besides the varying lithium content, which directly influences the amount of oxygen vacancies at ambient temperatures, possibly resulting in structural defects, such as stacking faults, which can significantly impact the thermal stability of the NCA structure.[33,37] Furthermore, the remaining composition of the structure influences the stability of the NCA cathode as well. While increasing nickel content has a destabilizing effect on the structure (promoting the rock salt structure),[26] the cobalt in NCA contributes to stability as it shifts the phase transition to higher temperatures.[24] This suggests that the high concentration of nickel in NCA layered transition metal oxides facilitates thermal degradation, while the introduction of cobalt and aluminum cations compensates for this effect.[38] Furthermore, aluminum contributes to the structural integrity by inhibiting the formation of highly charged O1 phase domains, slowing down the reduction of transition metals, such as cobalt, as shown by ref. [39]. The observed phase transitions from a stable layered structure at room temperature toward the rock salt

Research Article
doi.org/10.1002/batt.202500421
Chemistry Europe
European Chemical Societies Publishing

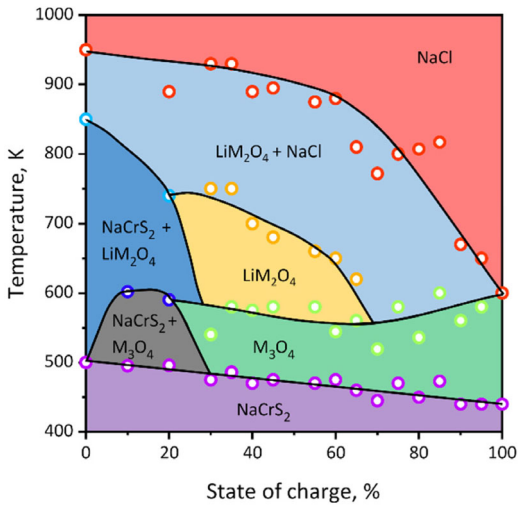

Figure 3. Temperature-composition phase diagram for NCA electrodes at different SOCs, showing the phase stability of differently delithiated NCA cathode structures.

structure at high temperatures can be summarized in a phase diagram represented in **Figure 3**.

The thermal stability at low temperatures was further tested using high-resolution X-ray diffraction. Measurements were carried out on the entire range of delithiated NCA cathodes, from 180 to 300 K (Figure S8, Supporting Information), where the NCA structure showed thermal stability in the entire studied range, with no evidence of phase transitions. That is, the $(003)_L$ reflection of the NCA structure in a charged state, typically representing the less stable state of the NCA structure, shows a systematic shift toward lower q at higher temperatures, illustrating thermal expansion in the c lattice direction during the heating. The $(104)_L$ reflection displays consistent behavior, which confirms that the NCA structure remains thermodynamically stable at low temperatures, irrespective of its delithiation state (SOC). Such behavior was confirmed by lattice parameter calculations based on the $(003/104)_L$ reflections (Figure S9, Supporting Information), showing similar stable behavior to the refined parameters across the whole SOC range at 300 K (Figure S6, Supporting Information). However, below 280 K, additional long-range order reflections were observed for the delithiated NCA structure. The reflections, as previously identified in literature,[16,28] are attributed to the freezing of residual electrolyte components that persist after the extraction of the cathode material from the battery cells. The exposure to low temperatures suggests that the remaining electrolyte components undergo a phase transition to a crystalline state, i.e., freezing. While low temperatures impact the properties of the liquid electrolyte in modern commercial LIBs, the integrity of the structural stability of delithiated NCA structures is not influenced, but shows thermal expansion of the structure. Thus, the linear thermal expansion coefficient α_L was calculated for temperature-dependent lattice parameters ($L = c$-/a-parameter, c/a, and unit cell volume) at various SOC, quantifying how lattice dimensions change with temperature. While α_a remained largely linear across defined temperatures and SOCs, α_c showed a significant SOC dependence, peaking between 50% and 80% SOC. This behavior reflects structural changes related to lithium de-/intercalation, particularly the change of interlayer spacing along the c-axis (Figure S10, Supporting Information). Furthermore, thermal expansion trends are similar to previously reported entropy changes,[40–43] both exhibiting a nonmonotonic variation across SOC. These correlations are explained via the Grüneisen parameter, linking thermal expansion, lattice vibrations, and entropy. The observations imply that both entropy and thermal expansion are driven by shared changes in the lattice dynamics and the electronic structure during electrochemical cycling. The findings highlight the important role of the cathode in influencing the thermodynamic behavior within full-cell LIBs.

3. Conclusion

The thermal degradation of differently delithiated NCA cathode materials is investigated in detail by a combination of powder diffraction techniques and thermal analysis, revealing the complex structural stability of the material at different SOCs. A complex interplay of cation migration, oxygen release, and phase transitions leads to a variety of degradation mechanisms. The NCA materials display a series of transformations starting from a stable layered $NaCrS_2$-type structure at ambient conditions to spinel phases (M_3O_4-type and LiM_2O_4-type), followed by a transition to a rock salt phase at higher temperatures. Both transition temperature and sequence are strongly influenced by the SOC, lithium and transition metal, and aluminum content. Higher SOCs and increased nickel content reduce thermal stability due to void formation and increased nickel and cobalt oxidation. While nickel and cobalt contribute to higher energy capacity, their destabilizing influence on structure stability at elevated temperatures represents an inevitable trade-off between performance and safety. Contrary, aluminum, which is electrochemically inactive, serves as a structural stabilizer by inhibiting the migration of cations and the formation of highly charged oxygen species, preserving lattice integrity under thermal stress. This trade-off between capacity and safety underscores the importance of composition optimization in cathode material development. Both TGA and DTA revealed that the extent of oxygen release and phase transition temperatures depend on the lithium content. Fully lithiated NCA (SOC 0%) demonstrates superior thermal stability with a single-step phase transition to the rock salt phase, while SOC $\geq$ 20% exhibits a two-step degradation process involving spinel intermediates. The stabilizing effect of lithium ions, combined with a lower amount of oxygen vacancies, the suppression of structural defects and the incorporation of aluminum highlights potential pathways for enhancing safety while mitigating performance losses. Additionally, high-resolution X-ray diffraction measurements confirm the structural transitions and the role of specific cations in stabilizing the NCA framework. Low-temperature tests further validate the structural integrity across all SOCs, with no evidence of phase transitions in the 180–300 K temperature range.

In summary, a characterization of the thermal stability of NCA-type cathodes is reported. The obtained results unambiguously

indicate the need to balance the advantages of higher capacity offered by increased nickel and cobalt content against the potential safety risks of reduced thermal and chemical stability. Alternatively, enhancing safety by increasing aluminum content will lower capacity but can play a positive role in thermal resilience, which in turn, may create a solid foundation for designing next-generation NCA-based cathodes with improved performance, safety, and stability for LIBs in high-energy applications.

4. Experimental Section

Electrode materials were extracted from fresh (formed) commercially available cylindrical LIBs of ICR18650 GA (Panasonic) type, possessing an NCA|C cell chemistry. The battery cells belong to a high-energy class, with gravimetric/volumetric energy densities of 224 Wh kg^{-1} and 693 Wh L^{-1},[44] a nominal voltage of 3.6 V, and nominal capacities of 3350 mAh. Electrochemical cycling was carried out (for the reactivation of the cells after storage) in the voltage range of 2.5–4.2 V, using a constant current of C/8 and a constant voltage with a cutoff current of C/100. After cycling, the cells were charged to specific predefined SOCs, between SOC 0%, corresponding to the lithiated state of the NCA structure, and SOC = 100%, corresponding to the delithiated state of the NCA structure. The electrodes were unrolled, separated, extracted, and ground to a fine powder in an argon atmosphere. Note: the cathode materials were extracted along with the anodes, reported in ref. [16].

A series of high-energy X-ray powder diffraction measurements was carried out at the beamline P02.1 at Petra III synchrotron (DESY, Hamburg, Germany), temperature-dependent. The experiment was carried out in Debye-Scherrer geometry, using a monochromatic beam with a size of $1 \times 1\ mm^2$ and a fixed wavelength $\lambda = 0.207$ Å (60 keV photon energy).[45] The exposure time was 60 s per pattern; the high-resolution configuration was chosen with a sample-to-detector distance of 2.25 m and a 2D Varex XRD 4343CT detector, possessing a 2880×2880 pixel area with a pixel size of $150 \times 150\ \mu m^2$. The NIST LaB_6 660c was used as a reference. Radial integration and data reduction were done with the Python library pyFAI.[46,47] For thermal treatment of the samples, an Oxford hot air blower was used for high temperatures (300–1000 K), and an Oxford Cryostream was used for subambient temperatures (180–300 K). The samples were placed in the sample magazine of the automatic sample exchanger, carried out by a robotic arm.

Simultaneous thermal analysis, combining TGA and DTA, was carried out on a Netzsch STA 449C Jupiter at the Institute of Inorganic Chemistry (Stuttgart, Germany). The samples were placed in Al_2O_3 crucibles, which were loaded in an argon-filled glovebox (O_2 and H_2O <1 ppm). To protect the samples from air, a lid with only a small hole was placed on the crucibles, and the samples were transferred from the glovebox to the measuring device in a closed glass bottle. Immediately after the transfer of the sample to the device, a vacuum cycle was started, and subsequently, the sample chamber was flooded with argon. This way air exposure of the sample was kept at a minimum. The measurements were carried out between 300 and 1000 K, applying a heating rate of 5 K min^{-1}.

Acknowledgements

The authors gratefully acknowledge the financial support provided by the Heinz Maier-Leibnitz Zentrum (Technical University of Munich), German Federal Ministry of Education and Research (BMBF project 05K19VK3). The authors thank DESY (Hamburg, Germany), a member of the Helmholtz Association HGF, for the provision of experimental facilities. Parts of this research were carried out at Petra III, P02.1 beamline. Beamtime was allocated for proposal I-20220351.

Open Access funding enabled and organized by Projekt DEAL.

Conflict of Interest

The authors declare no conflict of interest.

Data Availability Statement

The data that support the findings of this study are available from the corresponding author upon reasonable request.

Keywords: Nickel-Cobalt-Aluminum oxide cathodes · phase transitions · thermal analyses · thermal degradation · X-ray diffraction

[1] F. M. N. U. Khan, M. G. Rasul, A. S. M. Sayem, N. K. Mandal, *J. Energy Storage* **2023**, *71*, 108033.
[2] L. Westphal, V. Kochetov, V. Baran, T. Hölderle, M. Avdeev, V. Diadkin, K. Marshall, A. Schökel, K. Opri, R. Niewa, F. Porcher, P. Müller-Buschbaum, A. Senyshyn, *J. Phys. Chem. C* **2025**, *129*, 11546.
[3] B. Flamme, G. Rodriguez Garcia, M. Weil, M. Haddad, P. Phansavath, V. Ratovelomanana-Vidal, A. Chagnes, *Green Chem.* **2017**, *19*, 1828.
[4] T. Hölderle, D. Petz, V. Kochetov, V. Baran, A. Kriele, Z. Hegedüs, U. Lienert, M. Avdeev, P. Müller-Buschbaum, A. Senyshyn, *Energy Storage Mater.* **2025**, *75*, 104042.
[5] K. Nikgoftar, A. K. Madikere Raghunatha Reddy, M. V. Reddy, K. Zaghib, *Batteries* **2025**, *11*, 123.
[6] X. Zuo, J. Zhu, P. Müller-Buschbaum, Y.-J. Cheng, *Nano Energy* **2017**, *31*, 113.
[7] A. Manthiram, *Nat. Commun.* **2020**, *11*, 1550.
[8] K. Mizushima, P. C. Jones, P. J. Wiseman, J. B. Goodenough, *Mater. Res. Bull.* **1980**, *15*, 783.
[9] J. B. Goodenough, K. Mizushima, T. Takeda, *Jpn. J. Appl. Phys.* **1980**, *19*, 305.
[10] S. Chen, Z. Gao, T. Sun, *Energy Sci. Eng.* **2021**, *9*, 1647.
[11] S.-T. Myung, F. Maglia, K.-J. Park, C. S. Yoon, P. Lamp, S.-J. Kim, Y.-K. Sun, *ACS Energy Lett.* **2017**, *2*, 196.
[12] P. Hou, H. Zhang, X. Deng, X. Xu, L. Zhang, *ACS Appl. Mater. Interfaces* **2017**, *9*, 29643.
[13] T. Hölderle, M. Monchak, V. Baran, O. Dolotko, S. Bette, D. Mikhailova, A. Voss, M. Avdeev, H. Ehrenberg, P. Müller-Buschbaum, A. Senyshyn, *J. Power Sources* **2023**, *564*, 232799.
[14] B. Cui, Z. Xiao, S. Cui, S. Liu, X. Gao, G. Li, *Electrochem. Energy Rev.* **2024**, *7*, 27.
[15] A. Tomaszewska, Z. Chu, X. Feng, S. O'Kane, X. Liu, J. Chen, C. Ji, E. Endler, R. Li, L. Liu, Y. Li, S. Zheng, S. Vetterlein, M. Gao, J. Du, M. Parkes, M. Ouyang, M. Marinescu, G. Offer, B. Wu, *eTransportation* **2019**, *1*, 100011.
[16] T. Hölderle, M. Monchak, V. Baran, A. Kriele, M. J. Mühlbauer, V. Dyadkin, A. Rabenbauer, A. Schökel, H. Ehrenberg, P. Müller-Buschbaum, A. Senyshyn, *Batteries Supercaps* **2024**, *7*, e202300499.
[17] M. Guilmard, L. Croguennec, C. Delmas, *Chem. Mater.* **2003**, *15*, 4484.
[18] K.-W. Nam, S.-M. Bak, E. Hu, X. Yu, Y. Zhou, X. Wang, L. Wu, Y. Zhu, K.-Y. Chung, X.-Q. Yang, *Adv. Funct. Mater.* **2013**, *23*, 1047.
[19] M. M. Thackeray, C. Wolverton, E. D. Isaacs, *Energy Environ. Sci.* **2012**, *5*, 7854.
[20] J. B. Goodenough, Y. Kim, *Chem. Mater.* **2010**, *22*, 587.
[21] M. Armand, J. M. Tarascon, *Nature* **2008**, *451*, 652.
[22] K.-W. Nam, W.-S. Yoon, X.-Q. Yang, *J. Power Sources* **2009**, *189*, 515.
[23] S.-K. Jung, H. Kim, S. H. Song, S. Lee, J. Kim, K. Kang, *Adv. Funct. Mater.* **2022**, *32*, 2108790.

[24] S.-M. Bak, E. Hu, Y. Zhou, X. Yu, S. D. Senanayake, S.-J. Cho, K.-B. Kim, K. Y. Chung, X.-Q. Yang, K.-W. Nam, *ACS Appl. Mater. Interfaces* **2014**, *6*, 22594.
[25] N. Yabuuchi, T. Ohzuku, *J. Power Sources* **2003**, *119–121*, 171.
[26] S.-M. Bak, K.-W. Nam, W. Chang, X. Yu, E. Hu, S. Hwang, E. A. Stach, K.-B. Kim, K. Y. Chung, X.-Q. Yang, *Chem. Mater.* **2013**, *25*, 337.
[27] O. Dolotko, A. Senyshyn, M. J. Mühlbauer, K. Nikolowski, H. Ehrenberg, *J. Power Sources* **2014**, *255*, 197.
[28] A. Senyshyn, M. J. Mühlbauer, O. Dolotko, H. Ehrenberg, *J. Power Sources* **2015**, *282*, 235.
[29] H. Liu, H. Liu, I. D. Seymour, N. Chernova, K. M. Wiaderek, N. M. Trease, S. Hy, Y. Chen, K. An, M. Zhang, O. J. Borkiewicz, S. H. Lapidus, B. Qiu, Y. Xia, Z. Liu, P. J. Chupas, K. W. Chapman, M. S. Whittingham, C. P. Grey, Y. S. Meng, *J. Mater. Chem. A* **2018**, *6*, 4189.
[30] I. Hamam, R. Omessi, M. Ball, J. R. Dahn, *J. Electrochem. Soc.* **2024**, *171*, 060515.
[31] L. Wang, T. Maxisch, G. Ceder, *Chem. Mater.* **2007**, *19*, 543.
[32] M. Guilmard, L. Croguennec, D. Denux, C. Delmas, *Chem. Mater.* **2003**, *15*, 4476.
[33] H. Zhang, H. Liu, L. F. J. Piper, M. S. Whittingham, G. Zhou, *Chem. Rev.* **2022**, *122*, 5641.
[34] J. Rodríguez-Carvajal, *Phys. B* **1993**, *192*, 55.
[35] I. A. Bobrikov, N. Y. Samoylova, S. V. Sumnikov, O. Y. Ivanshina, R. N. Vasin, A. I. Beskrovnyi, A. M. Balagurov, *J. Power Sources* **2017**, *372*, 74.
[36] T. Li, X.-Z. Yuan, L. Zhang, D. Song, K. Shi, C. Bock, *Electrochem. Energy Rev.* **2020**, *3*, 43.
[37] H. Zhou, C. Zhang, S. Gong, Y. Sun, S. Guan, Y. Gao, P. Gao, Y. Zhu, S. Lou, X. Li, *J. Colloid Interface Sci.* **2025**, *698*, 138129.
[38] A. Dianat, N. Seriani, M. Bobeth, G. Cuniberti, *J. Mater. Chem. A* **2013**, *1*, 9273.
[39] E. Jo, J.-H. Park, J. Park, J. Hwang, K. Y. Chung, K.-W. Nam, S. M. Kim, W. Chang, *Nano Energy* **2020**, *78*, 105367.
[40] F. Friedrich, S. Pieper, H. A. Gasteiger, *J. Electrochem. Soc.* **2021**, *168*, 120502.
[41] Y. Gan, Z. Wu, H. Ye, S. Li, Y. Li, F. Liu, C. Xie, *Proc. Comput. Sci.* **2023**, *224*, 371.
[42] L. Spitthoff, M. S. Wahl, J. J. Lamb, P. R. Shearing, P. J. S. Vie, O. S. Burheim, *Batteries* **2023**, *9*, 249.
[43] J. Sun, Q. Ma, R. Liu, T. Wang, C. Tang, *Int. J. Energy Res.* **2019**, *43*, 7672.
[44] W. Diao, C. Kulkarni, M. Pecht, *Energies* **2021**, *14*, 5434.
[45] A.-C. Dippel, H.-P. Liermann, J. T. Delitz, P. Walter, H. Schulte-Schrepping, O. H. Seeck, H. Franz, *J. Synchrotron Radiat.* **2015**, *22*, 675.
[46] G. Ashiotis, A. Deschildre, Z. Nawaz, J. P. Wright, D. Karkoulis, F. E. Picca, J. Kieffer, *J. Appl. Crystallogr.* **2015**, *48*, 510.
[47] J. Kieffer, V. Valls, N. Blanc, C. Hennig, *J. Synchrotron Radiat.* **2020**, *27*, 558.

Manuscript received: May 30, 2025
Revised manuscript received: July 4, 2025
Version of record online: